Erschienen in: Chemistry : A European Journal ; 6 (2000), 2. - S. 385-393
https://dx.doi.org/10.1002/(SICI)1521-3765(20000117)6:2%3C385::AID-CHEM385%3E3.0.CO;2-A

Surfactant-Encapsulated Clusters (SECs): $(DODA)_{20}(NH_4)[H_3Mo_{57}V_6(NO)_6O_{183}(H_2O)_{18}]$, a Case Study

Dirk G. Kurth,[a]* Pit Lehmann,[a] Dirk Volkmer,[b] Helmut Cölfen,[a] Michael J. Koop,[b] Achim Müller,[b] and Alexander Du Chesne[c]

Abstract: We present a comprehensive study of the partially reduced polyoxomolybdate $[H_3Mo_{57}V_6(NO)_6O_{183}(H_2O)_{18}]^{21-}$ encapsulated in a shell of dimethyldioctadecylammonium (DODA) surfactant molecules. Treatment of an aqueous solution of $(NH_4)_{21}[H_3Mo_{57}V_6(NO)_6O_{183}(H_2O)_{18}]\cdot 65\,H_2O$ (**1a**) with a trichloromethane solution of the surfactant leads to instant transfer of the encapsulated complex anion into the organic phase. Results from vibrational spectroscopy, analytical ultracentrifugation, small-angle X-ray scattering, transmission electron microscopy, elemental analysis, and Langmuir compression isotherms are consistent with a single polyoxometalate core encapsulated within a shell of 20 DODA molecules. The molar mass of the supramolecular assembly is 20249 g mol^{-1} and the diameter is 3.5 nm. A material with the empirical formula $(DODA)_{20}(NH_4)[H_3Mo_{57}V_6(NO)_6O_{183}(H_2O)_{18}]$ (**2**) was isolated as a dark violet solid, which readily dissolves in organic solvents. Slow evaporation of solutions of **2** on solid substrates forces the hydrophobic particles to aggregate into a cubic lattice. Annealing these so-formed films at elevated temperature causes de-wetting with terrace formation similar to liquid crystals and block copolymers. Compound **2** forms a stable Langmuir monolayer at the air–water interface; Langmuir–Blodgett multilayers are readily prepared by repeated transfer of monolayers on solid substrates. The films were characterized by optical ellipsometry, Brewster angle microscopy, transmission electron microscopy, and X-ray reflectance.

Introduction

Transition metal polyoxoanions play a key role in areas such as catalysis, corrosion protection, electrochemistry, colloid chemistry, electroless deposition, lithography, and metallic patterning. In recent years, polyoxometalate chemistry has developed rapidly to produce an ever increasing number of structurally well-defined solid architectures. Although the formation pathways starting from aqueous solutions of simple metal oxide precursors to giant polyoxometalate clusters are not yet known in detail, a variety of polyoxometalates have been used in chemical synthesis as versatile building blocks for the construction of large supramolecular structures and inorganic materials. Some further attention has been devoted to the exploration of composite materials combining polyoxometalates with organic donor molecules. These materials possess a variety of interesting conducting, magnetic, electronic, and photonic properties.[1]

From a general point of view, our work aims at understanding how complex, yet well-defined materials assemble from simple starting materials through a series of growth and recognition processes. An intriguing example for such complex step-wise growth processes is the condensation of molybdate in acidic aqueous solutions in the presence of reducing agents; this leads to large anionic clusters.[2] Depending on the particular reaction conditions, a variety of nanosized polyoxomolybdates have been characterized as structurally well-defined solids over the past five years.[3] A representative example of this novel class of polyoxomolybdates is the compound $(NH_4)_{21}[H_3Mo_{57}V_6(NO)_6O_{183}(H_2O)_{18}]\cdot 65\,H_2O$ (**1a**).[4]

The progress achieved in polyoxometalate synthesis has not been matched, however, by a corresponding development in

[a] Dr. D. G. Kurth, Dipl.-Chem. P. Lehmann, Dr. H. Cölfen,
Max-Planck-Institute of Colloids and Interfaces
Golm, 14424 Potsdam (Germany)
Fax: (+49) 331-5679202
E-mail: kurth@mpikg-golm.mpg.de

[b] Dr. D. Volkmer, Dipl.-Chem. M. J. Koop, Prof. A. Müller
Universität Bielefeld, Anorganische Chemie 1
D-33501 Bielefeld, Postfach 100 131 (Germany)
E-mail: dirk.volkmer@uni-bielefeld.de

[c] Dr. A. Du Chesne
Max-Planck-Institut für Polymerforschung, Postfach 3148
D-55021 Mainz (Germany)
E-mail: duchesne@mpip-mainz.mpg.de

polyoxometalate surface chemistry. Modifying the chemical properties of surfaces of polyoxometalates opens new avenues to tailor their compatibility with organic materials and biological tissue. Controlled passivation of the cluster surface can be used to direct particle growth in synthesis and to stabilize clusters for handling and applications. In addition, multi-component composite materials can be fabricated by assembling functional components on polyoxometalates. The redox state of an individual cluster may be altered more efficiently and more selectively if it is encapsulated within an organized environment, a strategy which in nature is exemplified by a variety of proteins bearing multi-metal active sites (e.g., iron–sulfur proteins, ferritines).[5] Therefore, we launched an interdisciplinary program with the intention to attain a better understanding of the chemical properties of surfaces and to explore the surface chemistry of polyoxometalates as a tool to construct large supramolecular assemblies.

Commonly in cluster synthesis, surface modification relies on the exchange of labile ligands that are coordinatively bound to the peripheral metal atoms of the cluster resulting in either a chemical derivative or a rearranged cluster core. Examples for such strategies in polyoxometalate chemistry have only recently been reported. The terminal oxygen atoms of the hexamolybdate unit $[Mo_6O_{19}]^{2-}$ were partially or completely replaced by phenylimido ligands,[6] or the Keggin anion α-$[PMo_{12}O_{40}]^{3-}$ was treated with *p*-tolylisocyanate to yield a phenylimido-substituted polyoxometalate with a rearranged cluster core.[7] These modifications require prolonged reaction times under rather vigorous reaction conditions and suffer from low yields.

In contrast, the strategy that we present in this article relies on a ligand-exchange process in the second coordination sphere: the counter cations from the anions' hydration sphere are replaced by suitable alkylammonium surfactants; this results in discrete supramolecular entities. We were prompted to explore this approach by the successful endeavor to incorporate polyoxometalate clusters in polyelectrolyte multilayer films.[8] This colloid chemical approach has been successfully used in the past to stabilize a variety of semiconductor and precious metal nanoparticles,[9] but has never been applied convincingly to polyoxometalate chemistry.[10]

In the following, we describe the detailed characterization of **1a** and a novel surfactant-polyoxometalate assembly $(DODA)_{20}(NH_4)[H_3Mo_{57}V_6(NO)_6O_{183}(H_2O)_{18}]$ (**2**) in solution and in thin films.

Abstract in German: *In einer umfassenden Studie präsentieren wir das partiell reduzierte Polyoxomolybdat $[H_3Mo_{57}V_6(NO)_6O_{183}(H_2O)_{18}]^{21-}$, das in einer Schale von oberflächenaktiven Dimethyldioktadecylammonium-Ionen eingeschlossen ist. Ausschütteln einer wäßrigen Lösung von $(NH_4)_{21}[H_3Mo_{57}V_6(NO)_6O_{183}(H_2O)_{18}]\cdot 65\ H_2O$ (**1a**) mit einer Lösung der Tensidmoleküle in Chloroform führt zur Einkapselung und zum sofortigen Transfer des komplexen Anions in die organische Phase. Die Ergebnisse aus schwingungsspektroskopischen Untersuchungen, analytischer Ultrazentrifugation, Kleinwinkelröntgenbeugung, Transmissionselektronenmikroskopie, Elementaranalyse und Langmuir-Kompressionsisothermen zeigen übereinstimmend, daß ein isoliertes Polyoxometallat-Ion in einer Schale aus 20 DODA-Molekülen vorliegt. Die Molekülmasse des supramolekularen Aggregats beträgt 20249 g mol^{-1}, bei einem Durchmesser von ca. 3.5 nm. Aus der Chloroformlösung wurde ein dunkelviolettes Material gewonnen, das in organischen Solventien sehr gut löslich ist und dem eine empirische Summenformel $(DODA)_{20}(NH_4)[H_3Mo_{57}V_6(NO)_6O_{183}(H_2O)_{18}]$ (**2**) zugeschrieben wird. Beim langsamen Eindampfen der Lösungen von (**2**) aggregieren die hydrophoben Partikel in einer kubisch dichten Packung. Tempern der so erhaltenen Filme führt zur Entnetzung, wobei eine Terrassierung auftritt, ähnlich jener von Flüssigkristallen und Blockcopolymeren. Die Substanz (**2**) bildet eine stabile Monoschicht an der Wasser-Luft-Grenze, aus der sich durch wiederholten Transfer nach der Langmuir-Blodgett-Technik leicht Multischichten auf feste Substrate übertragen lassen. Die erhaltenen Filme wurden durch optische Ellipsometrie, Brewster-Winkel-Mikroskopie, Transmissionselektronenmikroskopie und Röntgenbeugung charakterisiert.*

Results and Discussion

Preparation of the surfactant-encapsulated cluster (SEC) 2: The surfactant-encapsulated polyoxometalate cluster **2** is assembled in a straightforward way by extracting an aqueous solution of polyoxometalate **1a** with DODA·Br into an arbitrary organic solvent. The SEC is immiscible in water, but readily dissolves in organic solvents such as benzene, toluene, or chloroform. In contrast, **1a** is only soluble in water. Experiments with different surfactants show that the micellization process is sensitive to steric factors of the tenside: trimethylhexadecylammonium bromide and methyltrioctadecylammonium bromide failed to completely transfer the inorganic cluster into the organic phase.

Elemental analysis established a composition of the SEC of $(DODA)_{20}(NH_4)[H_3Mo_{57}V_6(NO)_6O_{183}(H_2O)_{18}]$. Based on the single-crystal X-ray structure analysis, **1a** possesses 21 ammonium ions and, in addition, three acidic protons, that is, they balance a total of 24 negative charges. Since the number of DODA molecules is considered definite, an ammonium cation was introduced into the molecular formula to compensate the 21 negative charges of the cluster anion. Although the applied methods do not allow us to unambiguously detect a single ammonium cation in such a large assembly, this is a reasonable postulate: the center of the cluster anion bears a cavity suitable for binding an ammonium cation. In fact, the cavity with its preorganized oxygen electron pairs resembles the binding site of ammonium-binding crown ethers (see Figure 11 later).[11]

Spectroscopic investigations: Vibrational spectroscopy is the method of choice to prove the presence of the polyoxomolybdate anion $[H_3Mo_{57}V_6(NO)_6O_{183}(H_2O)_{18}]^{21-}$ (**1b**) in the final surfactant-encapsulated assembly. In solution, both **1b** and the surfactant-encapsulated cluster **2** show a strong band at 880 cm^{-1} and a weak shoulder at 955 cm^{-1}. The Raman spectrum of the starting material $(NH_4)_{12}[Mo_{36}(NO)_4O_{108}$-

$(H_2O)_{16}$] for the synthesis of **1a** also shows Raman bands at 885 (s) and 955 (vs) cm^{-1}, but with a different intensity ratio. The starting material also shows characteristic IR absorption bands at 619 and 773 cm^{-1}, which are absent in the spectrum of **2** (KBr pellets). The presence of starting material in **2** can, therefore, be ruled out. Further evidence arises from the UV-visible spectra of compounds **1a** and **2** which are almost identical. Compound **1a** shows an absorption band at 559 nm ($\varepsilon = 18000\ L\,mol^{-1}\,cm^{-1}$), and compound **2** shows a slightly shifted but similarly intense band at 568 nm ($\varepsilon = 16100\ L\,mol^{-1}\,cm^{-1}$). Vibrational (IR and Raman) and NMR spectroscopy of **2** confirm the presence of DODA. The ^1H NMR signals of the methyl groups are broadened and shifted downfield by 0.2 ppm; apparently, the surfactant is oriented with the positively charged head towards the negatively charged cluster surface.

Analytical ultracentrifugation (AUC): Analytical ultracentrifugation is an indispensable tool to obtain information on molar weights and size distributions of particles in solution. In the case of cluster **1a**, the electrostatic repulsion opposes the sedimentation of the particles and amounts to an incorrect molar mass. To screen the negative charges, sedimentation velocity measurements were carried out in the presence of excess electrolyte. The cluster sediments as an ideal species in 0.1N NH_4Cl. In this case, the sedimentation coefficient (s) is 4.81×10^{-13} s (25 °C). The corresponding diffusion coefficient calculated from the boundary spreading is $18.6 \times 10^{-7}\ cm^2\,s^{-1}$, which yields a molar mass of 10132 $g\,mol^{-1}$ from the Svedberg equation. Depending on the degree of dissociation and solvation in aqueous solution, the molar mass of a single cluster is expected to be within 10757 $g\,mol^{-1}$ (**1a**) and 9209 $g\,mol^{-1}$ (**1b**) based on the single crystal X-ray structure analysis.

The hydrodynamic diameter, which can be calculated from the diffusion coefficient, is 2.34 nm. From the particle size distribution (not shown), the hydrodynamic diameter was determined to be 2.24 ± 0.5 nm (11%).[12] Based on single crystal X-ray structure analysis, compound **1a** resembles a flattened ellipsoid with approximate dimensions of $a = b = 2.2$ nm, $c = 1.2$ nm; a spherical object with the same volume would hava a diameter of 1.8 nm. Taking into account the presence of a solvation sphere, the values for the molar mass and the diameter are consistent with single species.

The particles are also monodisperse, as demonstrated by the sedimentation velocity profiles. The profiles can be fitted to approximate solutions of the Lamm equation.[13] The sedimention boundary is very well described by the curve one expects for a monodisperse sample with a molar mass given above (Figure 1).

The sedimentation velocity experiments were independently confirmed by sedimentation equilibrium experiments as an absolute technique. Experiments were evaluated by two independent approaches. The first one uses the so-called M* function, which delivers a molar mass independent of any model.[14] The second approach makes use of a model-dependent fit of the equilibrium concentration gradient.[15] With the results obtained from sedimentation velocity ex periments, the model of monodisperse single species was applied. The apparent average molar weights $M_{w,app}$ of a

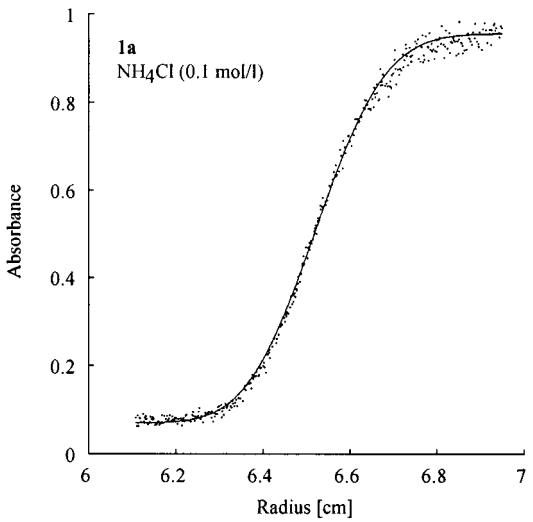

Figure 1. Theoretical (solid line) and measured (dots) sedimentation velocity profile for polyoxometalate **1a** as a function of the radial distance. The excellent agreement of theory and experiment confirms a monodisperse cluster of 10130 $g\,mol^{-1}$. (Here, the radius is the distance from the center of the centrifuge to the sedimentation boundary.)

concentration series are $10086 \pm 633\ g\,mol^{-1}$ for the first and $9868 \pm 964\ g\,mol^{-1}$ for the second method. Evidently, the assumption of an ideal monodisperse single species used in the second method is appropriate. The fits are of good quality as demonstrated in Figure 2, which is a representative example for the sedimentation equilibrium concentration gradient.

In contrast, analytical ultracentrifugation (AUC) measurements of **2** show that the particle sizes were strongly dependent on the particular solvent used in the measurement. This is illustrated in Figure 3. The particle size distributions show a

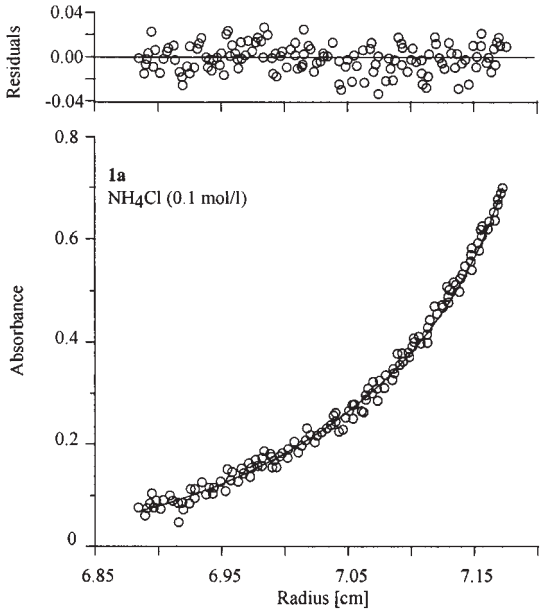

Figure 2. Representative example of the sedimentation equilibrium concentration gradient (open circles, bottom) fitted to the model of an ideal sedimenting species (solid line). The fit is of excellent quality (top: residuals of fit) indicating that the assumption of monodisperse species is justified. The concentration of **1a** was 0.16 $mg\,mL^{-1}$.

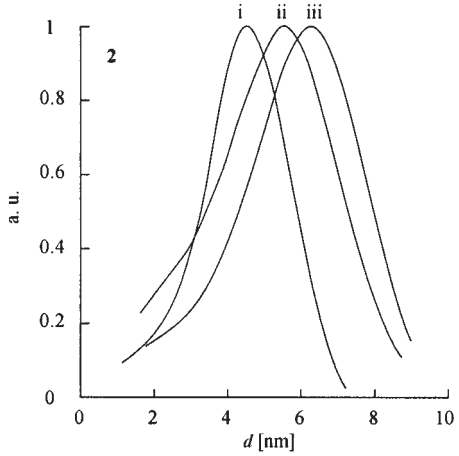

Figure 3. The particle size distribution of **2** depends on the solvent indicating aggregation. The graph shows results from sedimentation velocity measurements in i) THF, ii) toluene, and iii) cyclohexane.

tailing towards smaller species and are broader than that of **1a** (11 %). The average particle sizes exceed the expected size of single species of **2** (3.5 nm). The diameters in different solvents were determined to be: 3.92 ± 0.93 nm (24 %) in THF, 4.75 ± 1.34 nm (28 %) in toluene, and 5.53 ± 1.45 nm (26 %) in cyclohexane. The corresponding molar weights were determined to be 25 460 g mol^{-1}, 45 580 g mol^{-1}, and 71 850 g mol^{-1}, respectively. These results indicate that SECs aggregate in nonpolar solvents. Because chloroform has a similar density as **2**, it is not suitable for AUC measurements. As shown by SAXS (see below), the aggregates consist of individual SECs.

Small angle X-ray scattering (SAXS): Owing to the high electron density of the cluster anion **1b**, we used small angle X-ray scattering to examine the particle core. The experimental scattering intensities of **1a** and **2** are displayed in Figure 4 as a function of the scattering vector. From the similarity of the scattering functions, we immediately conclude that samples **1a** and **2** must be very similar. The solid lines are the computed scattering intensities for spherical

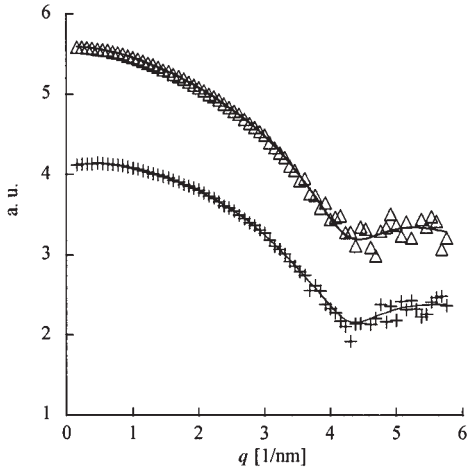

Figure 4. The experimental SAXS intensities of **1a** (+) and **2** (△). The solid lines are computed scattering intensities of homogeneous spheres of diameter 1.9 nm (**1a**) and 2 nm (**2**).

particles of 1.9 nm diameter (**1a**) and 2.02 nm (**2**).[16] The data confirm that the diameter of the polyoxometalate **1a** in solution and in the SEC directly correspond to the cluster core that was characterized in the single crystal X-ray structure analysis.

Thin films of SECs: Langmuir monolayers offer a simple and facile route to fabricate well-defined two-dimensional arrays of SECs. The compression isotherm of the monolayer is shown in Figure 5. We found that isotherms are very reproducible. Upon expansion, a slight hysteresis is observed; this is

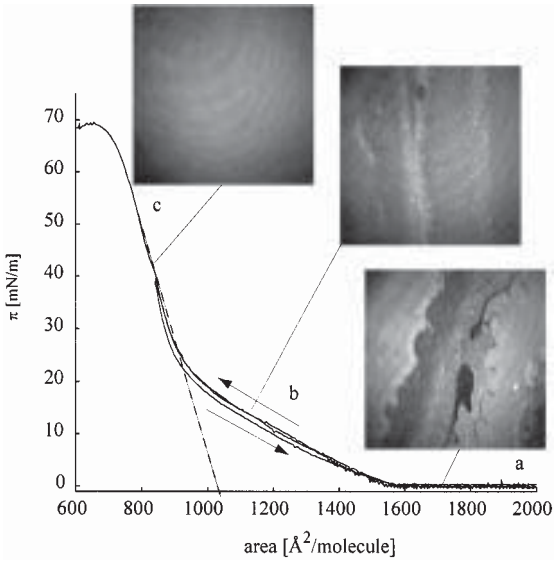

Figure 5. π-A isotherm, hysteresis (←compression, →expansion; target pressure 40 mN m^{-1}) and BAM images of **2** at the air–water interface. The hypothetical molecular area of **2** in the condensed phase was determined to be 10.4 nm^2 by interpolating the isotherm in the condensed-state region (c) to zero pressure (dashed line, a: gaseous state, b: expanded state). This value corresponds to an object with a diameter of 3.6 nm.

attributed to the tendency of **2** to aggregate. The hypothetical molecular area of **2** in the condensed phase (zero-pressure molecular area) was determined to be 10.4 nm^2 by interpolating the isotherm in this phase (region c) to zero pressure;[17] this corresponds to an object with a diameter of 3.6 nm. Based on the density of 1.04 g mL^{-1} for crystalline DODA · Br, one molecule occupies a volume of approximately 1 nm^3. Cluster **1a** has a surface area of approximately 19 nm^2; thus every DODA molecule can occupy a surface area of roughly 0.95 nm^2, which is a typical value for lipids in the liquid expanded phase.[18] A closed shell of DODA wrapped around the cluster would have a thickness of 1 nm. The total diameter of **2** is, therefore, estimated to be 3.8 nm. The molecular area is in good agreement with the estimated value for a single species of **2**.

Brewster angle microscopy (BAM, see inset Figure 5) shows that Langmuir monolayers of **2** are uniform. Large domains of uncharacteristic shape are seen in the gaseous phase (region a). Upon compression, the domains fuse in the liquid-expanded phase (region b). In the liquid-condensed phase (region c), **2** finally forms a continuous film, with a collapse pressure of 70 mN m^{-1}.

Multilayers of **2** were prepared by transferring monolayers from the air–water interface onto solid substrates with the Langmuir–Blodgett (LB) technique. Ellipsometry of the LB films on the solid substrate (Figure 6a) established a film thickness of 2.6 nm for the first layer and an average film

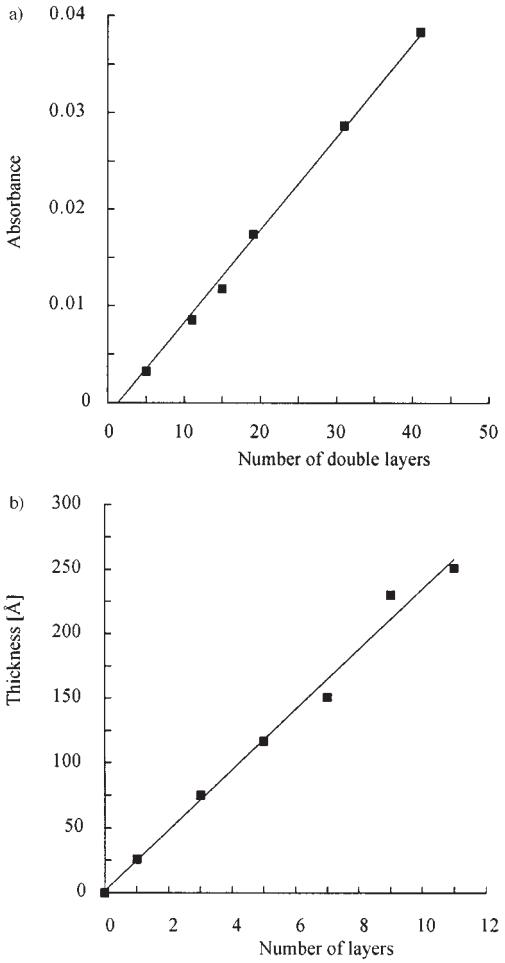

Figure 6. a) The ellipsometric thickness and b) the transmission UV/Vis absorption intensity at 570 nm of a LB film of **2** on a silicon wafer and a quartz wafer as a function of the number of layers. Clearly, a linear film growth is observed. The average thickness for one layer is 2.3 nm.

thickness of 2.3 nm for subsequent layers. These values are smaller than the diameter of the SEC, but packing effects within the film can reduce the apparent thickness per layer. Figure 6b also shows the increase of the absorption band at 570 nm of **2** on a quartz substrate as a function of the number of layers. Clearly, deposition is very reproducible and film growth is essentially linear, that is, in each dipping cycle equivalent amounts of SEC are transferred on the substrate (transfer ratio 0.95). The static contact angles of these surfaces were 102° for water and 31° for hexadecane in agreement with a highly hydrophobic surface. This demonstrates how efficiently the DODA layer screens the underlying hydrophilic cluster.

X-ray reflectivity of the LB multilayers on a silicon substrate shows well-resolved Kiessig fringes indicating a LB-film of uniform thickness (Figure 7). In addition, several Bragg reflections are discernible. This implies that the LB film

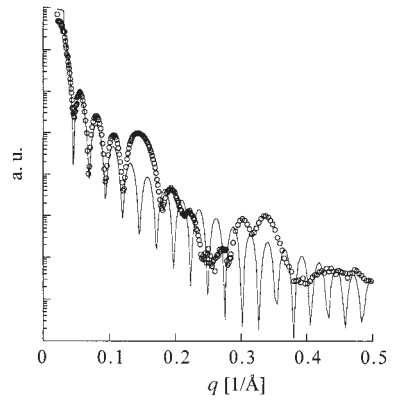

Figure 7. Experimental X-ray reflectance data (open circles) for a LB multilayer consisting of 11 layers of **2**. The sample shows nicely resolved Kiessig fringes and several Bragg peaks indicating a homogeneous film thickness and an internal structure. For comparison, a calculated reflectance curve (solid line) for a film with constant electron density and identical thickness (substrate: silicon) is shown.

has an internal layered structure. For comparison, Figure 7 also shows the calculated Kiessig fringes of a single layer of constant electron density and a thickness identical to that of the sample. It was not possible to fit the reflectance curves by a simple periodic electron density function and to retrieve the profile of the superlattice.[19] More insight into the structure of the thin films of **2** was obtained by transmission electron microscopy.

Transmission electron microscopy (TEM): Straightforward evidence for encapsulation is obtained by visualization of **2** by TEM. Figure 8 shows single clusters of **2** that form a

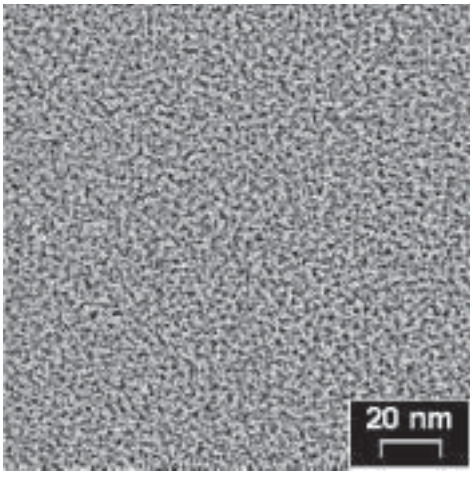

Figure 8. Thin film of **2** on a carbon-support film cast from a chloroform solution. Single clusters are clearly visible as dark dots with a diameter of 2 nm separated from one another by 3.8 nm (average distance determined by Fourier analysis).

monolayer on a supporting carbon film. The inorganic cores of the SEC appear as dark dots with diameters of 2 nm. The average center-to-center distance determined by Fourier analysis is 3.8 nm, in agreement with the size of **2** determined on the Langmuir trough.

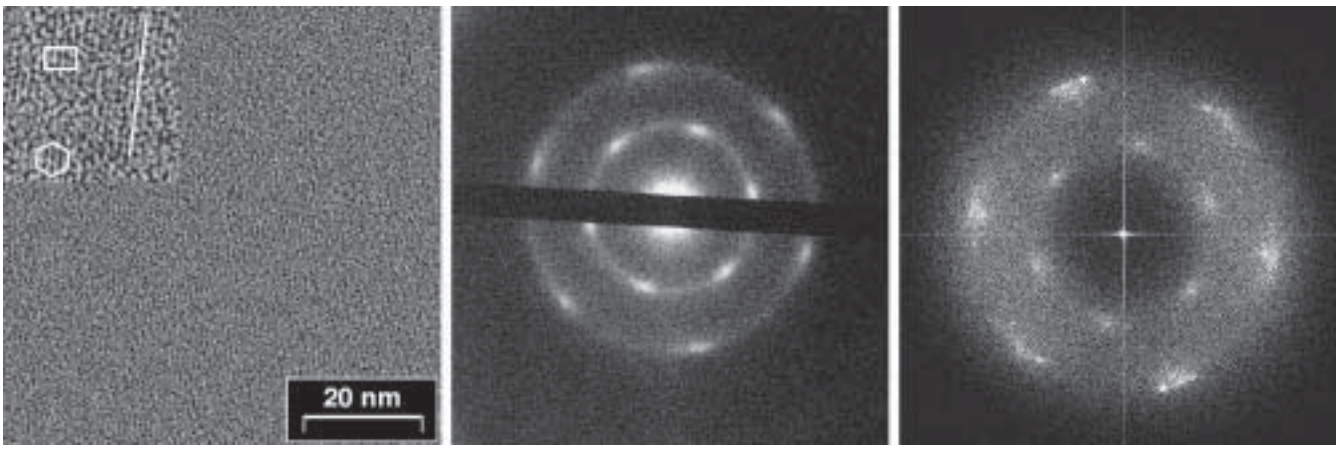

Figure 9. Left: Ordered region of an annealed film of **2**, recorded at 120 kV in the elastic filtering mode. The inset shows the six- and fourfold symmetry (width of inset = 50 nm). Middle: Elastically filtered electron diffraction pattern of the region shown in image at the left recorded at 120 kV (camera length 7.2 mm). The reflections are rather broad; this, according to the lefthand image, is due to slight local variations of spacings and orientation. The spacings encountered are 3.5 and 2 nm, the angle between the respective planes is 120°, angles between the two sets of planes are 60°. Right: Fourier spectrum calculated on the basis of the image on the left revealing threefold symmetry. The Fourier spectrum is in agreement with the electron diffraction pattern shown in the middle.

Thicker films of **2** revealed ordered domains. Figure 9 (left) displays a phase contrast image of such a film cast from chloroform solution and annealed for 15 h in vacuum at 50 K above the melting point of the surfactant. A sixfold axial symmetry is visible in Figure 9 (left, inset) that is consistent with a projection of a cubic lattice along [111] or of a hexagonal lattice along the *c* axis. Because inelastic electron scattering interferes the diffraction pattern, elastic filtering was applied.[20] The small-angle electron diffraction pattern of the region depicted in Figure 9 (middle) clearly shows reflections. Since the scattering centers are embedded in a mobile matrix, reflections are broad due to slight local variations of spacings and orientations of the underlying lattice, which should be considered as liquid crystalline. The inner reflections correspond to 3.5 nm, the outer ones to 2 nm. The angle between the corresponding planes related to each set of reflections is 120°, and the angle between the two sets of planes is 60°. There are some regions of the specimen in which fourfold symmetry is also visible (Figure 9, left). The concurrent occurrence of both, four- and sixfold symmetry projections in the same specimen is a strong indication for a cubic lattice. Hence, the reflections are assigned to 110 (d_{110} = 3.5 nm) and 211 (d_{211} = 2 nm) of a cubic lattice. Since the 110 reflection is forbidden for a face-centered packing, a body-centered (BCC) or simple-cubic (SC) packing is more probable. Indeed, BCC packing is expected in block copolymers with spherical microphases.[21]

Figure 9 (right) shows the Fourier spectrum calculated from Figure 9 (left). The similarity with the electron diffraction pattern is indeed remarkable. An analysis of the Fourier spectrum does in fact yield information identical to the above.

Upon annealing, thin films of **2** de-wet the carbon substrate and form layered structures (terracing) as has also been shown for thin films of liquid crystals and of block copolymers.[22] Figure 10 (left) shows a partially de-wetted monolayer and represents an enlarged detail of Figure 10 (right) in which the terracing becomes visible.

Conclusion

We present here for the first time a facile and simple approach to modify the chemical properties of surfaces of polyoxometalates; this method relies on the replacement of the charge-balancing counter-cations from the outer sphere of the hydrated polyoxomolybdate by cationic surfactants.

The applied methods prove that aqueous solutions of **1a** consist of single, monodisperse species with a molar mass of

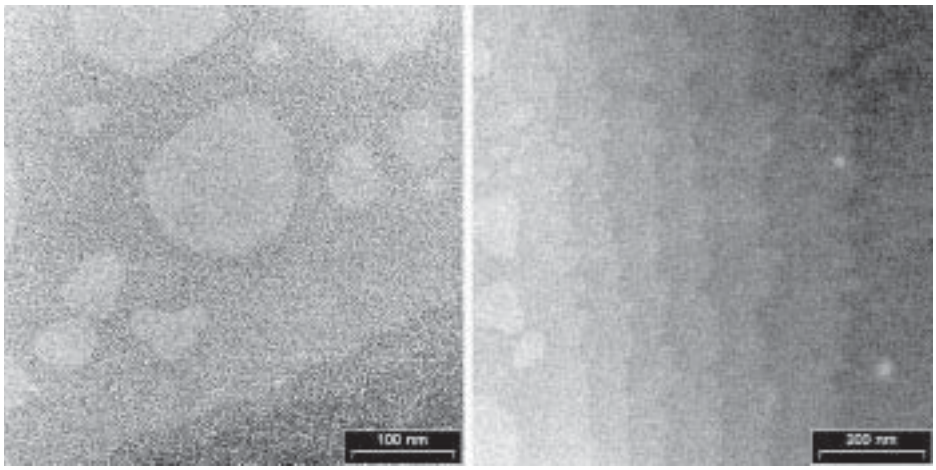

Figure 10. Electron micrograph of a thin film of SEC **2** recorded at 60 kV. Left: de-wetted regions are clearly discernible from regions densely covered by a monolayer. Right: overview of the same region demonstrating the terracing of **2** upon annealing.

10236 g mol^{-1}. The diameter of the polyoxomolybdate core is 1.9 nm and the hydrodynamic diameter is 2.3 nm. The surfactant-encapsulated cluster (SEC) **2** consists of a single polyoxomolybdate core (**1b**) and a shell of 20 DODA surfactant molecules. The diameter of **2** is 3.6 nm. The surfactant molecules are oriented with the positive head group towards the cluster anion. Depending on the solvent, the SEC has a tendency to form aggregates. Electrostatic binding is most likely the major driving force for encapsulation. These data are in excellent agreement with the expected values for single species based on the single crystal X-ray structure analysis of **1a**.

The surfactant-encapsulated cluster forms stable Langmuir monolayers at the air–water interface, and LB multilayers are readily transferred on solid substrates. The resulting LB films are completely hydrophobic; this demonstrates the efficient encapsulation of the hydrophilic cluster by the surfactant molecules. Also, by simple evaporation, SEC **2** forms highly ordered films. Upon annealing, the order of these film is improved; finally we observe de-wetting of the substrate and subsequent formation of terraced structures similar to liquid crystals and block copolymers. Some residual disorder in the length, small compared with the lattice parameters, remains in these films. This disorder could be due to random orientations of ellipsoidal polyoxometalate cores and/or slight deviations of their localization on the lattice sites. These degrees of freedom of the inner core are most likely provided by the mobile surfactant layer and might be useful for potential applications, for example, to align the inner cores by an external field at elevated temperature.

The whole assembly of cluster and surfactants on this level of structural organization resembles a reversed micelle in which the hydrophilic cavity is completely filled by the large cluster anion. A computer simulation of the SEC gives an idea of the packing of the surfactant molecules around the nano-sized cluster. The simulation in Figure 11 shows that up to 22 DODA molecules find accommodation on the cluster surface. More importantly, the cluster is completely shielded by the long hydrophobic tails of the octadecyl side chains; this explains the good solubility of the micelle-like clusters in organic solvents. Our experiments with different surfactants furthermore show that steric requirements and the balance of the hydrophobic/hydrophilic properties of the surfactants play an important role in stabilizing the structure of the surfactant-encapsulated clusters.

On-going experiments with different cluster/surfactant combinations lead us to assume that this approach should be generally suitable for the alteration of the surface properties of charged metal oxide colloids. Among these, polyoxomolybdates and polyoxotungstates with their well-defined molecular and electronic structures, the high surface-to-charge ratio, and their high stability are very promising candidates for the construction of nano-particulate composite materials with well-defined structures and predictable properties. For example, further functional groups may be introduced within the shell of amphiphilic molecules that may serve as recognition groups in biological or medical applications. The ability of polyoxometalates to undergo multiple reduction/oxidation steps may be exploited in information storage devices, electron transfer catalysts, or optical switches. The possibility to fabricate well-defined two-dimensional arrays is an important step towards this goal. Further work on polyoxometalates in organized matrices is in progress.

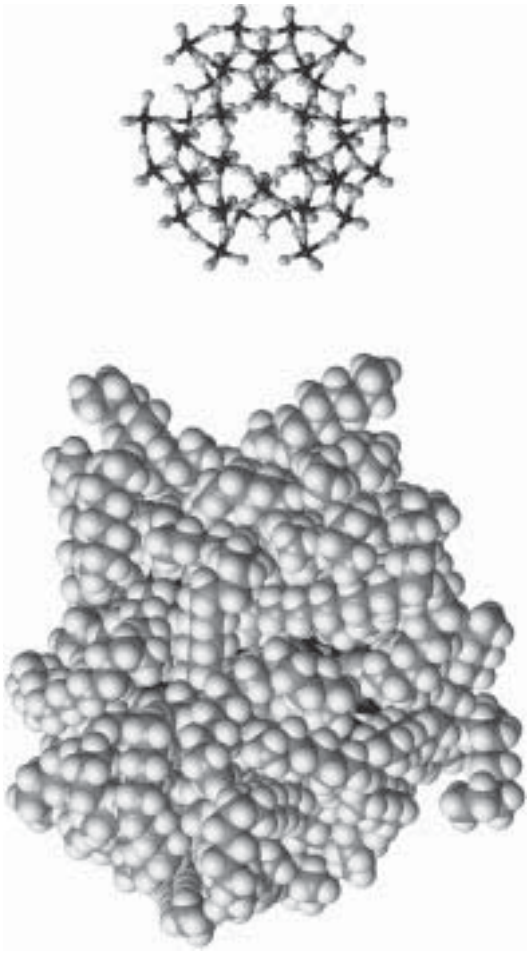

Figure 11. Ball-and-stick representation of the single crystal X-ray structure analysis of $[Mo_{57}V_6(NO)_6O_{183}(H_2O)_{18}]^{24-}$ (**1b**, top) and space-filling (hypothetical) computer model (bottom) of the surfactant-encapsulated cluster showing the complete shielding of the complex anion by the DODA molecules. For simplicity, three of the protons of **1** were omitted and a negative charge of 24 was used in the computation for $(DODA)_{22}[Mo_{57}V_6(NO)_6O_{183}(H_2O)_{18}]$.

Experimental Section

Preparation of 2: Samples of **2** were prepared by shaking a weighed sample of **1a** in aqueous HCl (pH 1.0) with a solution of dimethyldioctadecylammonium bromide (DODA · Br) in trichloromethane in stoichiometric or slightly less amounts. The complete transfer of the complex anion into the organic phase was indicated by the colorless aqueous phase. The phases were separated, and the trichloromethane solution was dried over anhydrous sodium sulfate. Solid samples of **2** were prepared by evaporating filtered solutions of chloroform to dryness and leaving the sample at 0.01 Torr until the weight remained constant. The density of **2** was measured with a DMA 602 instrument (Density Measuring Cell, Chempro/AutoM Paar KG) and was found to be 1.34 g mL^{-1}. Analysis by DSC (Mettler DSC 7) showed a phase transition at 17.5 °C, assigned to the melting of the C_{18} chains. Elemental analysis, NMR spectroscopy and ESCA were done at the Institut für Angewandte Chemie, Adlershof, Berlin. Dimethyldioctadecylammonium bromide (DODA · Br) was purchased from Fluka (99 %) and was used without further purification. IR:

$\tilde{\nu}$ = 2955, 2922, 2851, 1616, 1467, 980, 945, 885, 785, 719, 667, 611, 576, 560, 545 cm^{-1}; ^1H NMR (300 MHz, $CDCl_3$, 25 °C, TMS): δ = 0.88 (t, J = 7.02 Hz, 6H), 1.26 (br m, 4H), 1.68 (br m, 60H), 3.24 (br m, 6H), 3.52 (br m, 4H); UV/Vis ($CHCl_3$): λ_{max} (ε) = 570 nm (16100 L mol^{-1} cm^{-1}); $(N(C_{38}H_{80}))_{20}(NH_4)$-$[H_3Mo_{57}V_6(NO)_6O_{83}(H_2O)_{18}]$ (20249): calcd C 45.08, H 8.18, N 1.87, Mo 27.01, V 1.51; found C 45.25, H 8.54, N 1.67, Mo 27.52, V 1.55.

IR/Raman spectroscopy: Vibrational spectra were recorded with a Bruker FTIR IFS 66 instrument equipped with a FRA 106 Raman unit (Nd:YAG Raman laser excitation at 1064 nm). Samples for Raman spectra were dissolved in the appropriate solvent (1 mmol solutions, quartz cuvette, 1 cm optical path length). IR spectra were measured as KBr pellets in transmission.

UV/Vis spectroscopy: Spectra were measured with a Shimadzu UV-160A or a Cary 4E UV-VIS instrument (quartz cuvettes, 1 cm optical path length).The imaginary part of the refractive index was calculated from the UV/Vis spectrum and was found to be 0.0097 (ε (633 nm) = 12744 L mol^{-1} cm^{-1}).

Analytical ultracentrifugation: A Beckman Optima XL-I (Beckman Instruments, Palo Alto, USA) analytical ultracentrifuge equipped with an integrated scanning UV/Vis absorption and Rayleigh interference optical system was used for all measurements. Polyoxometalate **1a** was investigated at 25 °C in aqueous NH_4Cl solution (0.1 mol L^{-1}) at concentrations between 0.05 and 0.5 mg mL^{-1}. The detection wavelength was 560 nm, the applied speeds 20000 RPM for sedimentation equilibrium experiments and 60000 RPM for sedimentation velocity experiments. The density of the buffer solution was ρ = 1.01334 g mL^{-1} and the partial specific volume of the polyoxometalate **1a** was 0.369 mL g^{-1}. Sedimentation velocity experiments with **2** were performed at 25 °C in the solvents THF, cyclohexane, and toluene, all of HPLC grade. The detection wavelength and corresponding rotational speeds were 540 nm and 30000 RPM for toluene, 560 nm and 40000 RPM for cyclohexane, and 350 nm and 60000 RPM for THF.

Ellipsometry: Layer thickness was investigated with null ellipsometry using a Multiskop ellipsometer (Optrel, Germany, 2 mW HeNe Laser, 632.8 nm).

Brewster angle microscopy (BAM): BAM images were recorded with a BAM 1 plus Brewser Angle Microscope (Nanofilm Technology GmbH) equipped with a HeNe laser (632.8 nm) and a CCD camera.

Langmuir isotherm and preparation of LB multilayers: SEC **2** (226.4 mg) was dissolved in chloroform (25 mL, 5.22×10^{-5} mol L^{-1}). 100 μL of the solution were spread onto distilled water (Milli-Q water with a resistance higher then 18.2 MΩ cm) in a Lauda film balance. Deposition was performed on a Nima film balance by spreading 100 μL of a solution of **2** onto distilled water. The π-A isotherms were comparable in both cases, and were reproducible. Transfer was done at a constant surface pressure of 40 mN m^{-1} and a dipping speed of 0.6 cm min^{-1} (temperature 20 °C). The transfer ratio was always 0.95 ± 0.05 for both directions. The first layer was deposited during the upstroke. Silicon and glass wafers were used as substrates.[23] ESCA investigations of the deposited films confirmed the existence of the elements Mo, V, C, and N.

Small-angle X-ray diffraction: The experiments were done with a Kratky compact camera system that was equipped with a stepping motor and a counting tube with an impulse-height discriminator. The light source was a conventional X-ray tube with fixed copper target operating at 40 mA and 30 kV ($Cu_{K\alpha}$ = 0.154 nm). No monochromator (except the built-in impulse-height discriminator of the detector) was used. Instead, the Kβ contributions were numerically accounted for in the subsequent desmearing procedure which is included in the program ITP that transforms the scattering data into pair-distance distribution functions (PDDF).[24] Cluster **1a** was dissolved in aqueous 0.121N NH_4Cl at a concentration of 20.41 g L^{-1}; SEC **2** was measured in toluene at 26.91 g L^{-1}. Both samples were filtered through 20 nm pore-size filters directly into capillaries. The scattered intensities of the samples and of the solvents were recorded and subtracted from each other afterwards. Additional baseline contributions owing to incoherent scattering were subtracted so that the resulting PDDFs had an intercept of zero.

Transmission electron microscopy: Drops of the solutions (1 wt.%) were left to dry on 300 mesh copper grids coated with thin evaporated carbon films. Some of the **2** specimens were annealed under vacuum. Specimens were examined in a Leo EM 912 Ω. Images were taken using a SSCCD camera (14 bit, resolution 1024 × 1024) placed in the final image plane. An AnalySIS system (SIS) was used for data recording and image processing, which included Fourier analysis. The Leo EM 912 Ω was equipped with an imaging electron energy-loss spectrometer integrated into the TEM column.[25] This allows imaging of electrons with distinct energy loss. In the elastic filtering mode only elastically scattered and unscattered electrons contribute to the image. Hence, the resulting image is comparable with a conventional bright-field image, but may exhibit better contrast and higher resolution owing to lack of the effect of chromatic aberration.[26]

Molecular modeling: Molecular dynamics calculations were performed with the HyperChem 5.0 package. Atomic positions of the structure fragment $[Mo_{57}V_6(NO)_6O_{183}(H_2O)_{18}]^{24-}$ were extracted from the single crystal X-ray crystallographic data of compound **1a**. Partial charges were assigned as integer values to the corresponding metal centers. The ambiguous positions of the three acidic protons in the structure of **1a** were omitted thus leading to a total charge of −24 for the complex anion. Up to 22 dimethyldioctadecylammonium cations were subsequently introduced by molecular mechanics refinement steps (MM+ force field). The atomic positions of the complex anion were fixed during all calculations. The positions of the surfactant molecules around the micelle-like cluster were calculated by a molecular dynamics simulation of 20 ps equilibration time. Simulation started at 0 K and the temperature of the system was then allowed to reach 500 K within 5 ps. After a simulation period of 10 ps at 500 K the system was allowed to cool down to 0 K within 5 ps.

Acknowledgements

DGK and PL gratefully acknowledge financial support by the Max-Planck-Society; valuable discussions with Prof. H. Möhwald are greatly appreciated. DV thanks the Fonds der Chemischen Industrie for a Liebig fellowship. We thank John Philo and Amgen for providing the program Svedberg free of charge. The Deutsche Forschungsgemeinschaft is acknowledged for financial support. We thank H. Schnablegger for performing the small angle X-ray scattering measurements.

[1] For a recent overview on trends and applications in polyoxometalate chemistry see: *Chem. Rev.* **1998**, *98*, Issue 1 and references cited therein.

[2] a) A. Müller, J. Meyer, E. Krickemeyer, C. Beugholt, H. Bögge, F. Peters, M. Schmidtmann, P. Kögerler, M. J. Koop, *Chem. Eur. J.* **1998**, *4*, 1000; b) Mesopourous polyoxometalate materials are attainable through a hydrothermal process in the presence of surfactants; c) G. G. Janauer, A. Dobley, J. D. Guo, P. Zavalij, M. S. Whittingham *Chem. Mater.* **1996**, *8*, 2096; d) A. Taguchi, T. Abe, M. Iwamot *Adv. Mater.* **1998**, *10*, 667.

[3] a) A. Müller, W. Plass, E. Krickemeyer, S. Dillinger, H. Bögge, A. Armatage, A. Proust, C. Beugholt, U. Bergmann, *Angew. Chem.* **1994**, *106*, 897; *Angew. Chem. Int. Ed. Engl.* **1994**, *33*, 849; b). A. Müller, E. Krickemeyer, H. Bögge, M. Schmidtmann, C. Beugholt, P. Kögerler, C. Z. Lu, *Angew. Chem.* **1998**, *110*, 1278; *Angew. Chem. Int. Ed.* **1998**, *37*, 1220; c) A. Müller, E. Krickemeyer, H. Bögge, M. Schmidtmann, F. Peters, *Angew. Chem.* **1998**, *110*, 3567; *Angew. Chem. Int. Ed.* **1998**, *37*, 3360.

[4] For details on the single crystal X-ray structure analysis and the spectroscopic properties see: a) A. Müller, E. Krickemeyer, S. Dillinger, H. Bögge, W. Plass, A. Proust, L. Dloczik, C. Menke, J. Meyer, R. Rohlfing, *Z. Anorg. Allg. Chem.* **1994**, 599; b) D. Gatteschi, R. Sessoli, W. Plass, A. Müller, E. Krickemeyer, J. Meyer, D. Sölter, P. Adler, *Inorg. Chem.* **1996**, *35*, 1926.

[5] a) F. Capozzi, S. Ciurli, C. Luchinat, *Structure and Bonding* **1998**, *90*, 127; b) P. M. Harrison, P. D. Hempstead, P. J. Artymiuk, S. Andrews, *Met. Ions Biol. Syst.* **1998**, *35*, 435.

[6] a) J. B. Strong, R. Ostrander, A. L. Rheingold, E. A. Maatta, *J. Am. Chem. Soc.* **1994**, *116*, 3601; b) W. Clegg, R. J. Errington, K. A. Fraser, S. A. Holmes, A. Schäfer, *J. Chem. Soc. Chem. Commun.* **1995**, *455;* c) J. B. Strong, B. S. Haggerty, A. L. Rheingold, E. A. Maatta, *Chem. Commun.* **1997**, 1137.

[7] A. Proust, S. Taunier, V. Artero, F. Robert, R. Thouvenot, P. Gouzerh, *Chem. Commun.* **1996**, 2195.

[8] F. Caruso, D. G. Kurth, D. Volkmer, M. J. Koop, A. Müller, *Langmuir* **1998**, *14*, 3462.
[9] Representative examples for numerous studies are: a) Y. Tian J. H. Fendler, *Chem. Mater.* **1996**, *8*, 969; b) K. S. Mayya, V. Patil, M. Sastry, *J. Chem. Soc. Faraday Trans.* **1997**, *93*, 3377; c) J. R. Heath, C. M. Knobler, D. V. Leff, *J. Phys. Chem.* B **1997**, *101*, 189; d) G. Schmid, L. F. Chi, *Adv. Mater.* **1998**, *10*, 515; e) C. B. Murray, C. R. Kagan, M. G. Bawendi, *Science* **1995**, *270*, 1335; f) J. H. Fendler, F. C. Meldrum, *Adv. Mater.* **1995**, *7*, 607; g) X.Peng, T. E. Wilson, A. P. Alivisatos, P. G. Schultz, *Angew. Chem.* **1997**, *109*, 113; *Angew. Chem. Int. Ed. Engl.* **1997**, *36*, 145; h) J. R. Sachleben, V. Colvin, L. Emsley, E. W. Wooten, A. P. Alivisatos, *J. Phys. Chem.* B. **1998**, *102*, 10117.
[10] Mingotaud et al. studied the adsorption of heteropolytungstates of the Keggin type on a monolayer of DODA cations at the air–water interface and fabricated LB-multilayers: a) M. Clemente-León, B. Agricole, C. Mingotaud, C. J. Gómez-García, E. Coronado, P. Delhaès, *Langmuir* **1997**, *13*, 2340; b) M. Clemente-León, C. Mingotaud, B. Agricole, C. J. Gómez-García, E. Coronado, P. Delhaès, *Angew. Chem.* **1997**, *109*, 1143; *Angew. Chem. Int. Ed. Engl.* **1997**, *36*, 1114; c) M. Clemente-León, C. Mingotaud, C. J. Gómez-García, E. Coronado, *Thin Solid Films* **1998**, *329*, 439.
[11] M. M. N. Mautner, L. W. Sieck, J. F. Liebman, S. Scheiner, *J. Phys. Chem.* **1996**, *100*, 6445.
[12] The density of **1a** is 2.71 g mL^{-1}. The number in parenthesis is the standard deviation of the Gauss fit of the particle size distribution function.
[13] J. Philo, in *Modern Analytical Ultracentrifugation* (Eds.: T. M. Schuster, T. M. Laue), Birkhäuser, Boston, Basel, Berlin, **1994**, p. 156.
[14] a) H. Cölfen, S. E. Harding, *Eur. Biophys. J.* **1997**, *25*, 333; b) J. M. Creeth, S. E. Harding, *J. Biochem. Biophys. Methods* **1982**, *7*, 25.
[15] D. K. McRorie, P. J. Voelker, *Self-associating systems in the analytical ultracentrifuge*, Beckman Instruments, Palo Alto, California, **1993**.
[16] The ITP-software package was used (O. Glatter, *J. Appl. Cryst.* **1979**, *12*, 166, and references cited therein).
[17] This value is an average of five independent measurements.
[18] H. Möhwald, *Annu. Rev. Phys. Chem.* **1990**, *41*, 441.
[19] A. Asmussen, H. Riegler, *J. Chem. Phys.* **1996**, *104*, 8159.
[20] See Experimental Section; A. Du Chesne, *Macromolecular Chemistry and Physics* **1999**, *200*, 1813.
[21] E. L. Thomas, D. J. Kinning, D. B. Alward, C. S. Henkee, *Macromolecules* **1987**, *20*, 2934.
[22] a) Y. Bouligand, *J. Phys.* **1972**, *33*, 525; b) C. S. Henkee, E. L. Thomas , L. J. Fetters, *J. Mater. Sci.* **1988**, *23*, 1685; c) A. Du Chesne, G. Lieser, G. Wegner, *Coll. Polym. Sci.* **1994**, *272*, 1329.
[23] Substrates were cleaned according to: a) W. Kern *Semiconductor International* (April) **1984**, 94; b) K. Skidmore *Semiconductor International* (August) **1987**, 80.
[24] a) H. Schnablegger, O. Glatter, *Appl. Opt.* **1991**, *30*, 4889; b) H. Schnablegger, O. Glatter, *J. Colloid Interface Sci.* **1993**, *158*, 228; c) M. Kerker, *The Scattering of Light and Other Electromagnetic Radiation*, Academic Press, San Diego, **1969**.
[25] "Design of an Analytical TEM with Integrated Imaging Ω-Spectrometer", J. Bihr, G. Benner , D. Krahl , A. Rilk, E. Weimer, in *Proceedings of the 49th Annual Meeting of the Electron Microscopy Society of America* (Ed.: G. W. Bailey), San Francisco Press, **1991**, p. 354.
[26] Reimer L., in *Advances in Electronics and Electron Physics* (Ed.: P. W. Hawkes), Academic Press, Boston, **1991**, *81*, 67.